Materials Research Proceedings 41 (2024) 1779-1788 https://doi.org/10.21741/9781644903131-197

Surrogate modeling for multi-objective optimization in the high-precision production of LiDAR glass optics

VU Anh Tuan[1,a *], PARIA Hamidreza[1,b], GRUNWALD Tim[1,c] and BERGS Thomas[1,2,d]

[1]Fraunhofer Institute for Production Technology IPT, Aachen, Germany

[2]Manufacturing Technology Institute (MTI), RWTH Aachen University, Aachen, Germany

[a]anh.tuan.vu@ipt.fraunhofer.de, [b]hamidreza.paria@ipt.fraunhofer.de, [c]tim.grunwald@ipt.fraunhofer.de, [d]thomas.bergs@ipt.fraunhofer.de

Keywords: Nonisothermal Glass Molding, Glass Optics, LiDAR, Surrogate Modeling, Bayesian Optimization, Industry 4.0

Abstract. This study addresses the ever-increasing demands on glass optics for LiDAR systems in autonomous vehicles, highlighting the pivotal role of the recently developed Nonisothermal Glass Molding (NGM) in enabling the mass production of complex and precise glass optics. While NGM promises a significant advancement in cost- and energy-efficient solutions, achieving the requisite shape and form accuracy for high-precision optics remains a persistent challenge. The research focuses on expediting the development phase, presenting a methodology that strategically utilizes a sparse dataset for determining optimized molding parameters with a minimized number of experimental trials. Importantly, our method highlights the exceptional ability of a robust surrogate model to precisely predict the accuracy outputs of glass optics, strongly influenced by numerous input molding parameters of the NGM process. This significance emphasizes the surrogate model, which emerges as a promising alternative to inefficient traditional methods, such as time-consuming experiments or computation-intensive simulations, particularly in the realm of high-precision production for LiDAR glass optics. In contributing to optics manufacturing advancements, this study also aligns with contemporary trends in digitalization and Industry 4.0 within modern optics production, thereby fostering innovation in the automotive industry.

Introduction

The rapid evolution of autonomous vehicle technology has ushered in a new era of transportation, promising unprecedented safety and efficiency. At the forefront of this technological revolution is Light Detection and Ranging (LiDAR), a key sensing technology that enables vehicles to navigate and perceive their surroundings with remarkable precision. As LiDAR systems play a critical role in providing real-time, three-dimensional mapping of the vehicle's environment, the efficacy of the optical components is paramount to ensure accurate and rapid data acquisition. In the quest to enhance LiDAR systems, the focus on optical components has become pivotal, serving as a cornerstone for achieving heightened performance and reliability. Glass optics, known for outstanding mechanical strength, durability, and exceptionally high transparency, stands out as a compelling solution to meet the rigorous demands of LiDAR systems. Nevertheless, amidst the recent growth in LiDAR technology, glass optics manufacturers are facing rising demands, including increasing geometrical complexity, high form accuracy, surface roughness, exceptional optical functionalities, reduced energy consumption, and cost-effectiveness from the dynamic LiDAR market.

Addressing these challenges, the “Glass4AutoFuture” project at Fraunhofer IPT, Germany aimed to develop a cost- and energy-efficient manufacturing technology enabling the high-volume production of optical glass components essential for future car concepts. Nonisothermal Glass

Molding (NGM), a replication-based process, has emerged as a viable technology for manufacturing complex and precision glass optics on a mass production scale [1,2]. In NGM, a glass preform is compressed between two mold halves at high temperature, and after cooling, optics with the desired shape are achieved without additional post-processing steps like grinding and polishing [3]. With the ability to produce multiple optics in parallel and eliminating the need for postprocessing, NGM holds the potential for high-volume production [4].

Nevertheless, the primary challenge that remains with NGM technology is to achieve the desired shape and form accuracy required for high precision LiDAR optics. These characteristics are influenced by multiple factors, including highly nonlinear deformation behaviors arising from nonequilibrium viscoelasticity of glass, the heat transfers between glass and molding environments, and numerous forming parameters. Understanding the thermal-mechanical behaviors of glass during the forming process and optimizing the forming parameters are crucial to satisfy the requirements of the glass optics [5]. These tasks are far from trivial, given the multitude of parameters influencing the accuracy of the optics, making the process development through an experimental trial-and-error method inefficient.

This study presents a method for determining optimized molding parameters with a minimal number of experimental trials. The proposed solution involves the development of a robust surrogate model that enables the multi-objective optimization of glass molding process parameters using a sparse dataset. The procedure consists of two steps. First, a process simulation model was established, accounting for the highly nonlinear viscoelastic deformation behavior of glass and all heat transfer phenomena occurring in the forming process. The simulation model serves as a tool to generate data for developing the surrogate model. The subsequent step involves exploring different surrogate models, acquisition functions, and selection strategies to minimize iterations while converging to the global solution. The results demonstrate that the surrogate model accurately approximates the outputs features of the product quality, offering reliable estimations that can substitute the computationally expensive simulations or time-consuming experiments.

Optics demonstration and experimental setup

To demonstrate the methodology proposed in this study, an optical lens was purposefully designed for an optics demonstration. Fig. 1 presents the lens design and underlies the accuracy requirements for the demonstration. The design features a plano-convex lens commonly utilized for laser beam collimation in numerous LiDAR laser scanner systems. The precision of the optical lens is crucial for ensuring the high performance of the LiDAR system, as any single photon loss in the laser beam is unaffordable. Consequently, the form accuracies of the plane and spherical surfaces of the lens emerge as critical considerations. For this reason, *form deviation of the spherical surface and center thickness* were specifically identified as the primary criteria for optimizing the NGM process.

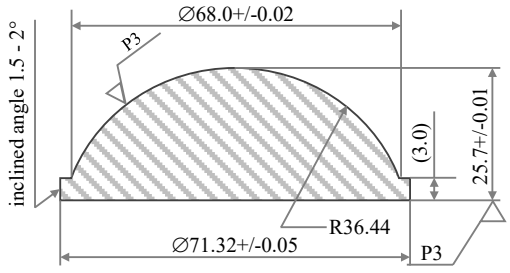

Material	B270i
Refractive index n_d	1.52308 +/- 0.001
Abbe number	58.57 +/- 0.0818
Birefringence	10 nm/cm
Specifications according to DIN ISO 10110	
Form accuracy	3/ 0.005
Center thickness	25.7 +/-0.01
Bubbles and other inclusions	1 / 3×0.16
Inhomogeneity and Striae	2 / 0;3
Surface imperfections	5 / 3×0.16

Fig. 1. Design and specifications of the optical demonstration.

Fig. 2 outlines the process chain, experimental setup, and the process diagram indicating the parameters designed for producing the chosen lens demonstration. In the initial step, multiple glass preforms were heated in an external oven, while the two mold halves were preheated at a constant temperature, referred to as the *mold temperature* (T_M). Once the preforms reached a predefined *glass temperature* (T_G), each preform was automatically transferred to the molding position by a robot arm. At this stage, the glass preform was compressed in the space between two mold halves at a constant *pressing velocity* (v), until a predefined *pressing force* (F), set to prevent glass breakage, was attained. The force was maintained for a certain period – the *pressing time* (t_H) – to allow for complete deformation of the glass into the mold cavity. Following the molding step, the molded glass optics were transferred to an annealing oven, where multiple molded glass lenses underwent sequential cooling steps, comprising three *cooling times* (C_{t_i}, *i=1-3*). Each cooling time was carefully defined to allow the release of stress remaining after the molding step, ultimately achieving the desired shape of the molded lens after cooling at room temperature.

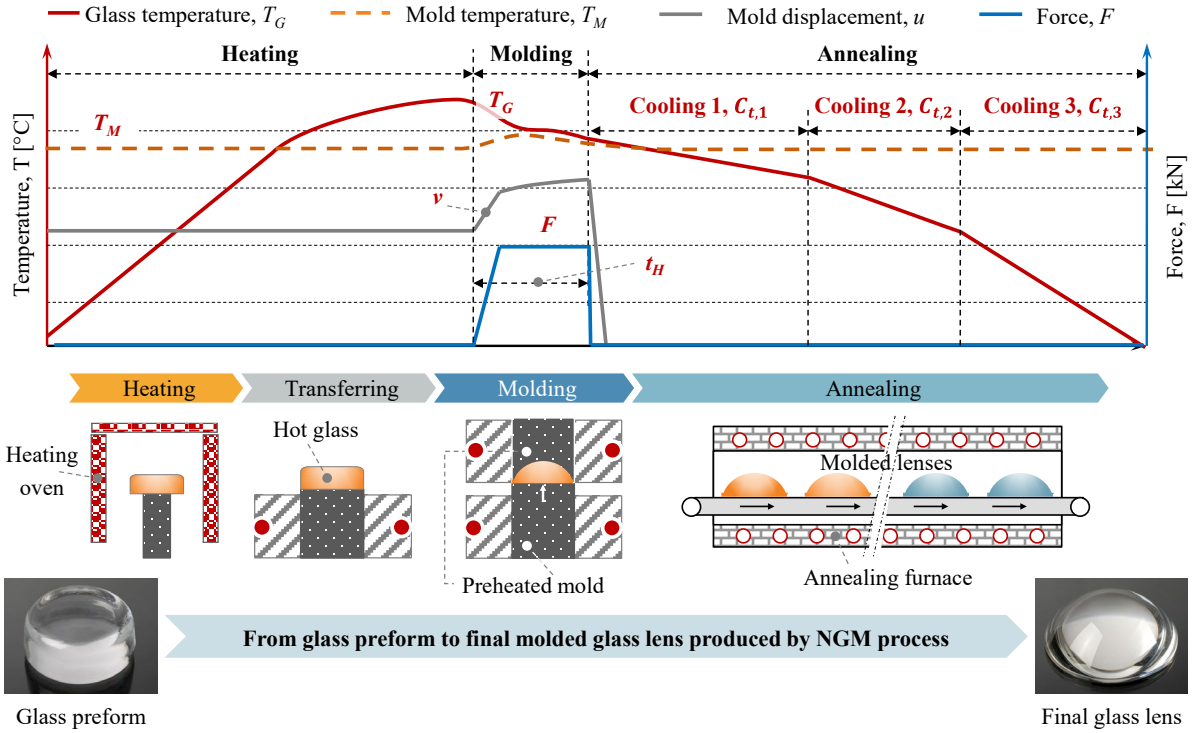

Fig. 2. Description of NGM process and the process parameters required for optimization.

Process modeling

As depicted in Fig. 2, the molding process involves a set of 8 parameters, comprising of the set temperature of glass for molding T_G, predefined mold temperature T_M, molding velocity v, pressing force F, molding time t_H, and three phases of cooling in an annealing furnace $C_{t,i}$ where $i = 1 - 3$. The product quality is highly sensitive to these parameters, where adjustments to individual parameters can cause significant alterations in the final shape and form accuracy of the molded lens. The sensitivity arises from the complex, nonlinear thermoviscoelastic behaviors exhibited by glass during the molding step [6–8], coupled with nonlinear shrinkage behaviors resulting from structural relaxation during the cooling step [9–11]. Consequently, the conventional trial-and-error method for adjusting process parameters is both demanding and labor-intensive.

To address these challenges, this study introduces a numerical modeling approach for the NGM process. The overall goal is to understand the correlation between the process parameters (inputs)

and the accuracy criteria (outputs), facilitating a multi-objective optimization method that minimizes the required dataset, given the computational expense of process simulation.

Fig. 3 presents the simulation model constructed to capture the thermal- and mechanical responses throughout the molding process. A coupled thermal-mechanical model was, therefore, necessary. The thermal model calculates the temperature distributions within the molding components, accounting for their thermal interactions with the molding environment. All relevant heat transfer phenomena at the boundaries, including convection and radiation, were considered. Convective and radiative heat transfer coefficients were defined through the utilization of infrared thermographic techniques, with the methodology and inverse heat transfer solution detailed in [12]. In addition, the heat transfer across the glass-mold interface, governed by the thermal contact conductance depending on the pressure p, interfacial temperature T, and surface roughness Ra, was adopted from prior works [13,14].

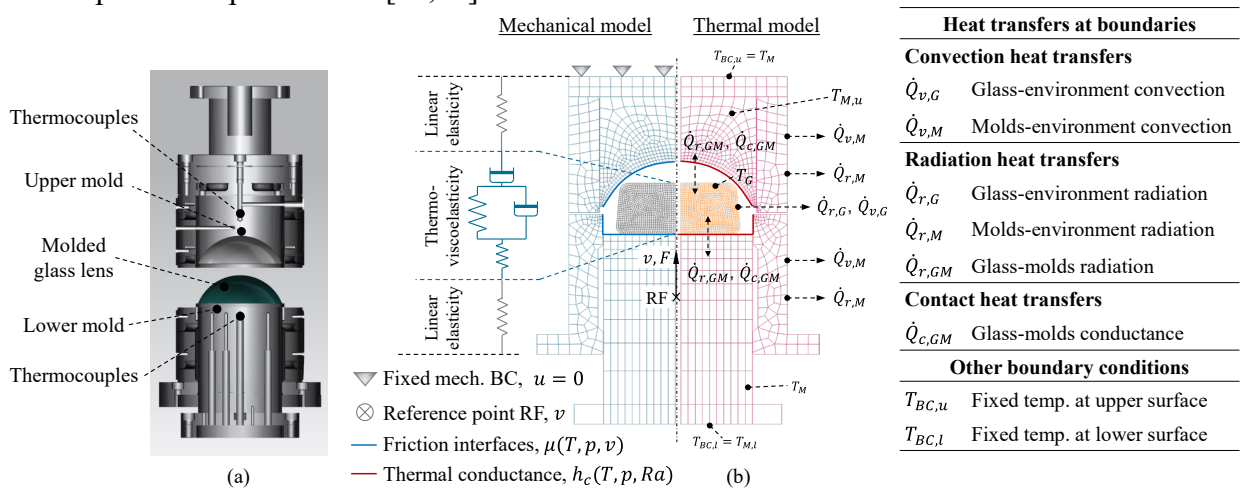

Fig. 3. (a) Setup and molding components, and (b) coupled thermal-mechanical model of the NGM process [12].

The mechanical model addresses the material responses of glass, including the stress relaxation and structural relaxation phenomena during molding and subsequent cooling. In the nonisothermal molding process, there are constantly heat exchanges at the glass surfaces with the colder molds and the molding environment, leading to a transition in the glass state from equilibrium to nonequilibrium [15]. Capturing the relaxation nature of the nonequilibrium glass necessitates a robust material model incorporating three variables: time, temperature, and thermal history [15]. A material model, developed in previous work [9], was adapted here to address the stress relaxation behaviors over the entire range of molding temperature, including thermo-viscoelasticity during the molding step and the shrinkage behaviors of glass due to the structural relaxation during the annealing step. Furthermore, the mechanical interaction at the glass-mold interface was modeled by a Coulomb's friction model. The friction coefficients, dependent on temperature T, pressure p, and sliding velocity v, were adopted from the previous work [16].

Methodology

Conventional optimization methods commonly rely on 1st or 2nd order gradients of objective function or employ bio-inspired optimization algorithms such as evolutionary algorithms, which necessitate a large number of objective function evaluations to identify the global solution. In contrast, Bayesian Optimization (BO) stands out as a derivative-free machine learning method that endeavors to comprehend the intricate black box function of the system with limited and sparse dataset availability. Notably, BO exhibits efficiency in handling objective functions containing diverse systematic noises.

Multi-Objective Bayesian Optimization (MOBO). The versatility of BO becomes evident in multi-objective optimizations (MOO), where it diverges from single-objective optimization algorithms. Instead of converging to a single solution, MOO using BO converges to the Pareto optimal set of solutions within the design space of input features. This is especially pertinent when dealing with conflicting objective features, where enhancing one feature inevitably leads to the degradation of others. The set of corresponding output values for the Pareto optimal solutions is referred to as the *Pareto Front* (PF) set for a collection of conflicting objective parameters [17,18].

Building on these principles, the present study employed a MOBO framework, illustrated in Fig. 4. It encompasses four key steps: an initial sampling method, the construction of a surrogate model, the definition of an acquisition function, and the implementation of a selection strategy. This holistic approach allows MOBO to effectively navigate the complexities inherent in multi-objective optimization scenarios.

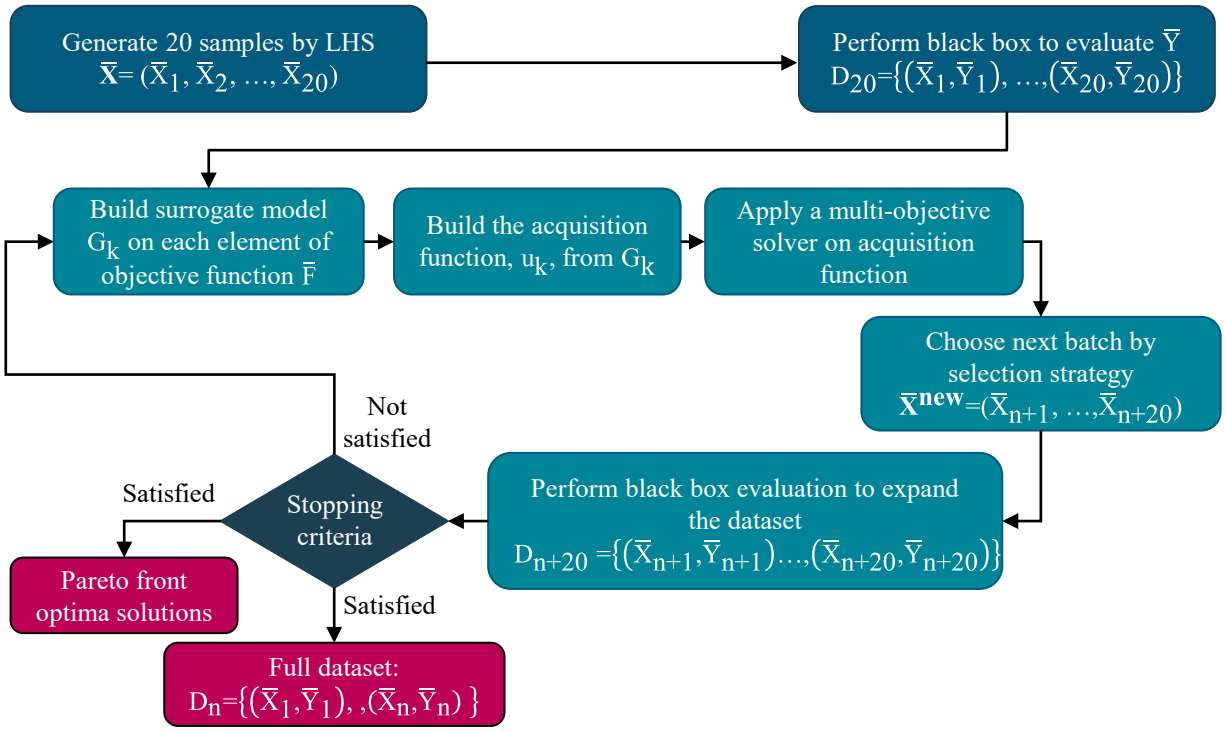

Fig. 4. Flowchart of the multi-objective Bayesian optimization.

Surrogate model. A surrogate model, a supervised machine learning approach, emulates complex and costly black box functions with high accuracy [19]. In this study, Gaussian Process (GP) was chosen among various supervised models like artificial neural networks (ANN) and tree-based methods due to its simplicity, fewer hyperparameters, and reduced sensitivity to the initial design of experiments [20]. GP proves advantageous in handling sparse datasets, avoiding overfitting issues that more complex models like ANN may encounter when trained on limited data. In this study, the GP surrogate model is trained independently for each objective parameter.

GP training: During the initial GP training on the black box function $\mathbf{f}$: $\Omega \rightarrow \mathbb{R}^k$ with "k" elements of objectives, and design space of $\Omega \in \mathbb{R}^d$, a prior model was defined by mean function $m(\bar{\mathbf{x}})$: $\Omega \longrightarrow \mathbb{R}$, and Matern kernel (covariance) function $k(\bar{\mathbf{x}},\bar{\mathbf{x}})$: $\Omega \times \Omega \longrightarrow \mathbb{R}$. This prior model was established without observing available data, forming a prior belief over the design space. For any given input variable $\bar{\mathbf{x}}$, the prior of GP was expressed as:

$$f(\bar{\mathbf{x}}) \backsim N(m(\bar{\mathbf{x}}), k(\bar{\mathbf{x}},\bar{\mathbf{x}})). \quad (1)$$

Posterior GP training: Subsequently, a posterior of the GP was trained to refine the prior model using the available dataset, $D_n = \{(\bar{\mathbf{X}}, \bar{\mathbf{Y}})\} = \{(\bar{X}_1, \bar{Y}_1), (\bar{X}_2, \bar{Y}_2), \dots, (\bar{X}_n, \bar{Y}_n)\}$ expressed as:

$$f(\bar{\mathbf{x}}) \backsim N(\mu(\bar{\mathbf{x}}), \sigma(\bar{\mathbf{x}})),\ \mu(\bar{\mathbf{x}}) = m(\bar{\mathbf{x}}) + \mathbf{k}\mathbf{K}^{-1}\bar{\mathbf{Y}},\ \sigma(\bar{\mathbf{x}}) = k(\bar{\mathbf{x}},\bar{\mathbf{x}}) - \mathbf{k}\mathbf{K}^{-1}\mathbf{k}^{T},$$

where $\mathbf{k}=k(\bar{\mathbf{x}}, \overline{\mathbf{X}})$, and $\mathbf{K} = k(\overline{\mathbf{X}}, \overline{\mathbf{X}})$. (2)

Details for the surrogate model, prior, and posterior functions are elaborated in [17,21,22].

Acquisition function: Once the surrogate model G_k was constructed to estimate each objective function f_k, $k \in \mathbb{N}$ on available dataset, the acquisition function, serving as a cost-effective function to evaluate, was simply defined using the mean $\mu(\bar{\mathbf{x}})$ and the uncertainty $\sigma(\bar{\mathbf{x}})$ of the posterior function of the surrogate model:

$$u(\bar{\mathbf{x}}|D_n) = u(\mu(\bar{\mathbf{x}}), \sigma(\bar{\mathbf{x}})). \quad (3)$$

The primary objective of the acquisition function is to suggest the most promising single or batch of samples to be added to the dataset in the next iteration. This involves striking a balance between *exploitation*, focusing on the region with the highest mean value of the negative objective $\mu(\bar{\mathbf{x}})$, and *exploration*, exploring areas with high objective function uncertainty $\sigma(\bar{\mathbf{x}})$. The global maximum solution of the acquisition function, representing the trade-off between exploitation and exploration, guides the selection of new samples in the next iteration:

$$\bar{x}^{new} = \arg\max_{\bar{x}\in\Omega} u(\bar{\mathbf{x}}|D_n). \quad (4)$$

Examples of well-known acquisition functions include Expected Improvement (EI), Probability of Improvement (PI), Upper Confidence Bound (UCB), and Thompson sampling [18]. In this study, the Identity function, simply equal to mean $\mu(.)$ of G_k, is used as an acquisition function.

Selection strategy: After deriving the optimum points from the acquisition function, there are two methods for selecting sample(s) for the next iteration of the algorithm: sequential selection and batch selection. In sequential selection, one optimum point is chosen as the candidate for the next iteration in each cycle. While limiting the number of newly added samples to the dataset, it results in a high number of algorithm iterations and a low convergence rate. In contrast, the batch selection method suggests a batch of samples, improving the convergence rate of the algorithm. This strategy is particularly suitable when the black box function can be evaluated in parallel.

Three established methods for choosing the batch of samples for the upcoming iteration of MOBO are Kriging Believer (KB), Local Penalization (LP), and Believer-Penalizer (BP) [20–22].

Results

The optimization process involves a set of 8 parameters. Table 1 provides an overview of the process parameters along with the selected range of physical constraints for each parameter. The table serves as a comprehensive reference, outlining the specific boundaries within which the MOBO framework operates to fine-tune the system and achieve optimal outcomes.

Automated optimization procedure. To automate the entire optimization procedure, the FEM model representing the entire NGM process, was treated as the black box function. This model, scripted in Python, seamlessly integrated with the MOBO algorithm. This integration allows the MOBO algorithm to generate any required simulation run through a simple command. The process parameters in Table 1 were defined as functional variables in Python, enabling the MOBO algorithm to efficiently modify and submit relevant simulations during its iterative runs. After each FEM simulation run's completion, essential output data was extracted from the .DAT file generated by ABAQUS and transmitted to MOBO as output parameter values.

Table 1. List of process parameters with their physical ranges defined for NGM process.

Parameter	Denotation	Unit	Lower bound	Upper bound
Glass temperature	T_G	[°C]	750.0	850.0
Molds temperature	T_M	[°C]	480.0	580.0
Molding velocity	v	[m/s]	1e-3	2e-2
Pressing force	F	[kN]	5.0	30.0
Pressing time	t_H	[s]	5.0	30.0
Cooling time 1	$C_{t,1}$	[s]	1800.0	18000.0
Cooling time 2	$C_{t,2}$	[s]	1680.0	168000.0
Cooling time 3	$C_{t,3}$	[s]	2742.0	13710.0

For MOBO implementation, the open-source Python library AutoOED was employed [21], and its hyperparameters were tuned following the methodology in [22]. The primary objective was to minimize two parameters of the black box function, representing the required accuracy criteria of the glass lenses. These objectives include: (i) optimizing the form accuracy of the molded lenses, quantified as the Root Mean Square Error (RMSE) of the convex surfaces between the desired shape y and that estimated by the FEM simulation $\hat{y}$, as per Eq. 5, and (ii) minimizing the absolute error between the center thickness of the lens and the target value given as 25.7 mm.

$$\text{RMSE}(\hat{\mathbf{y}}, \mathbf{y}) = \sqrt{\sum_{i=1}^{n} \frac{(\hat{y}_i - y_i)^2}{n}}. \quad (5)$$

As presented in Fig. 4, the MOBO algorithm commenced with the generation of 20 quasi-random sample distributions along each input feature using Latin Hypercube Sampling (LHS) [23], denoted as $\overline{\boldsymbol{X}}_{\mathbf{0}} = (X_1, X_2, \ldots, X_{20}) \in R^{20\times 8}$. These samples constituted the initial design space. After running 20 simulations for each input sample, the objective parameters were evaluated, resulting in $\overline{\mathbf{Y}}_{\mathbf{0}} = (Y_1, Y_2, \ldots, Y_{20}) \in R^{20\times 2}$, referred to as the initial performance space. With both the initial design and performance spaces created, the MOBO algorithm was initiated, and through each iteration, 20 new samples were added to the dataset. These samples underwent FEM simulation to obtain the associated output parameters. This process continued until one of the predefined stopping criteria was attained. Two stopping criteria were defined: the first criterion was satisfied if the form accuracy error and center thickness error reach values below 5 μm and 0.1 mm, respectively. The second criterion was when the total number of iterations reaches 10, equivalent to a dataset of 200 samples.

The output results for each iteration were visually represented in a performance space plot, where the objective features were plotted against each other. Fig. 5(a) exhibits the outcomes of the LHS, while Fig. 5 (b) illustrates the results of the MOBO after 7 iterations. The upper plots showcase the full performance spaces, and the lower plots zoom in on the rectangular region delineated by a dash-dot line in the upper plot. The green region in the lower left corner of both lower plots represents the area where the first objective criterion was fulfilled. The grey zones indicate areas where only one of the objective features satisfied the criterion, while the orange zone signifies that none of the targets were achieved. Given that 20 samples were generated in each iteration, Fig. 5(b) only shows the best sample achieved after each iteration, considering both objectives. This selected set is termed the *Pareto Front* (PF) for that specific iteration.

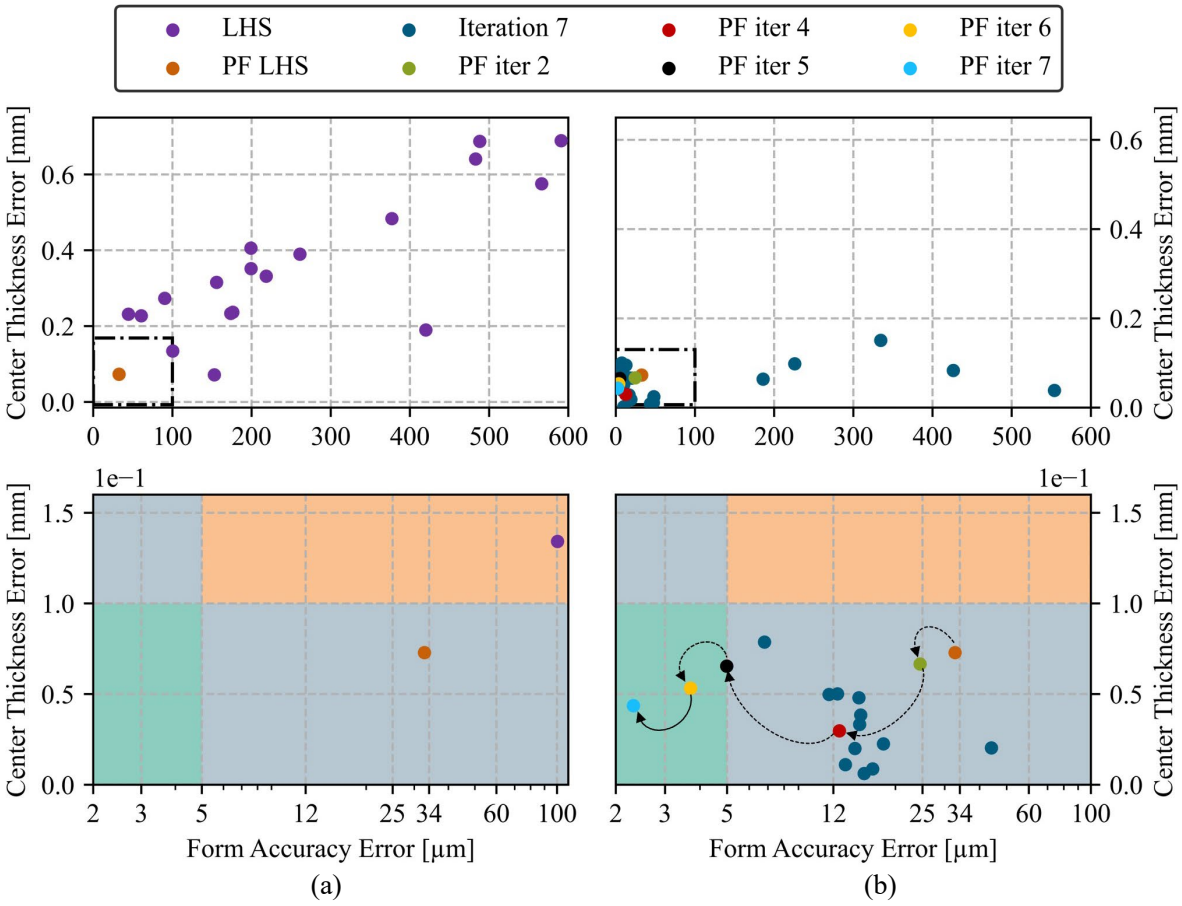

Fig. 5. Results of the MOBO algorithm on FEM simulation of the NGM process.

The inherent randomness of LHS is evident in Fig. 5(a), as data samples spread far from the defined target values, and only one best sample from the first generation is located in the grey zone. However, Fig. 5(b) demonstrates a significant improvement in objective values obtained by iteration 4, with the algorithm meeting the predefined criteria for the first time in iteration 5. Continuing for two more iterations, MOBO reveals that not only can global solutions be enhanced, but potential local minima in the design space can also be uncovered, thanks to its exploration and exploitation features. In iteration 7, 12 more samples lie in the grey zone, highlighting MOBO's capability not only in identifying global optimum points but also in intelligently designing experiments by detecting possible local minima, thus reducing the required number of data samples compared to conventional Design of Experiment (DoE) algorithms.

To assess the prediction accuracy of GP as the surrogate model in MOBO, the absolute error between the estimated and target values is given for each sample in Fig. 6. After 7 iterations, encompassing 160 samples including the initial LHS, the error plots for both output features nearly reach zero. The result reveals that with this sample size, *the surrogate model accurately approximates the output features, offering reliable estimations that can substitute the computationally expensive FEM simulations*. In addition, the GP prediction error significantly diminishes after generating 80 samples (4 iterations). This marks the first instance where MOBO detects the vicinity of the global optimum solution, as illustrated in Fig. 5. Despite slight fluctuations in the center thickness error plot during iteration 5, the algorithm effectively refines the global solution, emphasizing the robustness and efficacy of the MOBO methodology.

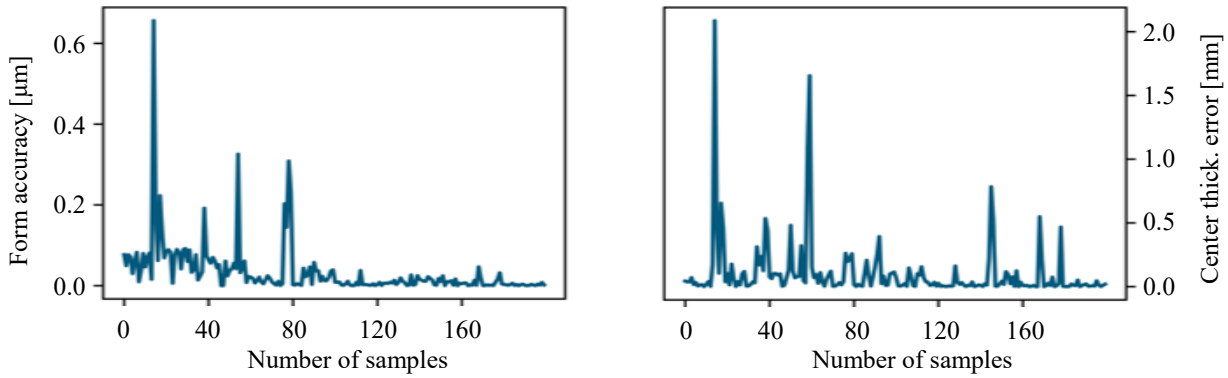

Fig. 6. The absolute error between the outputs predicted by Gaussian process and those given by FEM simulation.

Summary

Tackling the challenge of finding the global solution while minimizing operational time is a fundamental concern in optimizing processes with multiple variables, particularly in precision-demanding applications like glass molding. While experimental operations are time-consuming and labor-intensive, simulating glass molding processes requires huge computational resources. Our research enlightens the effectiveness of a MOBO framework as a surrogate model, offering an alternative approach to predict product accuracy based on multiple molding parameters. The methodology holds promising implications for industry applications. By conducting a limited number of trial experiments during the process development phase, industrial users can efficiently obtain optimized parameters aligned with specific product accuracy criteria, leading to accelerated phases of process development and production ramp-up. This study aligns with current trends in digitalization and Industry 4.0, contributing to innovation within the automotive industry.

Acknowledgement

This research was supported within the Fraunhofer and DFG transfer program under the project »Glass4AutoFuture«. Grant number: 032-600020.

References

[1] H. Kreilkamp, A.T. Vu, O. Dambon, N.F. Klocke, Non-Isothermal Glass Moulding of Complex Led Optics, in: S.K. Sundaram (Ed.), 77th Conference on Glass Problems, Wiley (2017) 141–149. https://doi.org/10.1002/9781119417507.ch13

[2] H. Kreilkamp, A.T. Vu, O. Dambon, F. Klocke, Replicative manufacturing of complex lighting optics by non-isothermal glass molding, in: D.H. Krevor, W.S. Beich, M.P. Schaub, A. Symmons (Eds.), Polymer Optics and Molded Glass Optics: Design, Fabrication, and Materials SPIE (2016) 99490B. https://doi.org/10.1117/12.2235848

[3] C. Strobl, P.A. Vogel, A.T. Vu, H. Mende, T. Grunwald, R.H. Schmitt, T. Bergs, Enabling Sustainability in Glass Optics Manufacturing by Wafer Scale Molding, KEM 926 (2022) 2371. https://doi.org/10.4028/p-hachrx

[4] A.T. Vu, H. Kreilkamp, O. Dambon, F. Klocke, Nonisothermal glass molding for the cost-efficient production of precision freeform optics, Opt. Eng 55 (2016) 71207. https://doi.org/10.1117/1.OE.55.7.071207

[5] A.T. Vu, H. Kreilkamp, B.J. Krishnamoorthi, O. Dambon, F. Klocke, A hybrid optimization approach in non-isothermal glass molding, in: Author(s) (2016) 40006.

[6] A.T. Vu, A.N. Vu, T. Grunwald, T. Bergs, Modeling of thermo-viscoelastic material behavior of glass over a wide temperature range in glass compression molding, J Am Ceram Soc 103 (2020) 2791–2807. https://doi.org/10.1111/jace.16963

[7] G. Liu, A.T. Vu, O. Dambon, F. Klocke, Glass Material Modeling and its Molding Behavior, MRS Advances 2 (2017) 875–885. https://doi.org/10.1557/adv.2017.64

[8] F. Wang, Simulating the precision glass molding process. Zugl.: Aachen, Techn. Hochsch., Diss., 2013, 1st ed., Apprimus-Verl., Aachen, 2014.

[9] A.T. Vu, T. Grunwald, T. Bergs, Thermo-viscoelastic Modeling of Nonequilibrium Material Behavior of Glass in Nonisothermal Glass Molding, Procedia Manufacturing 47 (2020) 1561. https://doi.org/10.1016/j.promfg.2020.04.350

[10] T.D. Pallicity, A.T. Vu, K. Ramesh, P. Mahajan, G. Liu, O. Dambon, Birefringence measurement for validation of simulation of precision glass molding process, J Am Ceram Soc 100 (2017) 4680–4698. https://doi.org/10.1111/jace.15010

[11] F. Wang, Y. Chen, F. Klocke, G. Pongs, A.Y. Yi, Numerical Simulation Assisted Curve Compensation in Compression Molding of High Precision Aspherical Glass Lenses, Journal of Manufacturing Science and Engineering 131 (2009). https://doi.org/10.1115/1.3063652

[12] A.T. Vu, Modeling Relaxation Nature of Nonequilibrium Glass in Nonisothermal Glass Molding. Dissertation, 2023.

[13] A.T. Vu, A.N. Vu, G. Liu, T. Grunwald, O. Dambon, F. Klocke, T. Bergs, Experimental investigation of contact heat transfer coefficients in nonisothermal glass molding by infrared thermography, J Am Ceram Soc 102 (2019) 2116–2134. https://doi.org/10.1111/jace.16029

[14] A.T. Vu, T. Helmig, A.N. Vu, Y. Frekers, T. Grunwald, R. Kneer, T. Bergs, Numerical and experimental determinations of contact heat transfer coefficients in nonisothermal glass molding, J Am Ceram Soc 103 (2020) 1258–1269. https://doi.org/10.1111/jace.16756

[15] A.T. Vu, R.d.l.A. Avila Hernandez, T. Grunwald, T. Bergs, Modeling nonequilibrium thermoviscoelastic material behaviors of glass in nonisothermal glass molding, J Am Ceram Soc 105 (2022) 6799–6815. https://doi.org/10.1111/jace.18605

[16] A.T. Vu, T. Grunwald, T. Bergs, Friction in Glass Forming: Tribological Behaviors of Optical Glasses and uncoated Steel near Glass Transition Temperature, J Non-Cryst Solids (2024).

[17] B. Shahriari, K. Swersky, Z. Wang, R.P. Adams, N. de Freitas, Taking the Human Out of the Loop: A Review of Bayesian Optimization, Proc. IEEE 104 (2016) 148–175. https://doi.org/10.1109/JPROC.2015.2494218

[18] S. Greenhill, S. Rana, S. Gupta, P. Vellanki, S. Venkatesh, Bayesian Optimization for Adaptive Experimental Design: A Review, IEEE Access 8 (2020) 13937–13948. https://doi.org/10.1109/ACCESS.2020.2966228

[19] S. Ranftl, W. von der Linden, Bayesian Surrogate Analysis and Uncertainty Propagation, in: The 40th International Workshop on Bayesian Inference and Maximum Entropy Methods in Science and Engineering, MDPI, Basel Switzerland (2021) 6. https://doi.org/10.3390/psf2021003006

[20] F. Mekki-Berrada, Z. Ren, T. Huang, W.K. Wong, F. Zheng, J. Xie, I.P.S. Tian et al., Two-step machine learning enables optimized nanoparticle synthesis, npj Comput Mater 7 (2021). https://doi.org/10.1038/s41524-021-00520-w

[21] Y. Tian, M.K. Luković, T. Erps, M. Foshey, W. Matusik, AutoOED: Automated Optimal Experiment Design Platform, arXiv, 2021.

[22] M.K. Luković, Y. Tian, W. Matusik, Diversity-Guided Multi-Objective Bayesian Optimization with Batch Evaluations, in: Proceedings of the 34th International Conference on Neural Information Processing Systems, Curran Associates Inc, Red Hook, NY, USA, 2020.

[23] P. Saves et al., SMT 2.0: A Surrogate Modeling Toolbox with a focus on hierarchical and mixed variables Gaussian processes, Advances in Engineering Software 188 (2024) 103571. https://doi.org/10.1016/j.advengsoft.2023.103571